Frontiers of Information Technology & Electronic Engineering
www.jzus.zju.edu.cn; engineering.cae.cn; www.springerlink.com
ISSN 2095-9184 (print); ISSN 2095-9230 (online)
E-mail: jzus@zju.edu.cn

Intertidal area classification with generalized extreme value distribution and Markov random field in quad-polarimetric synthetic aperture radar imagery*

Ting-ting JIN[†1,2], Xiao-qiang SHE[†‡1,3], Xiao-lan QIU[1], Bin LEI[1]

[1]*Key Laboratory of Technology in Geo-spatial Information Processing and Application System, Institute of Electronics, Chinese Academy of Sciences, Beijing 100190, China*

[2]*University of Chinese Academy of Sciences, Beijing 100049, China*

[3]*Huawei Software Technologies Co., Ltd., Nanjing 210012, China*

[†]E-mail: jintingting13@mails.ucas.ac.cn; sxq@mail.ustc.edu.cn

Received July 11, 2017; Revision accepted Aug. 28, 2017; Crosschecked Feb. 15, 2019

Abstract: Classification of intertidal area in synthetic aperture radar (SAR) images is an important yet challenging issue when considering the complicatedly and dramatically changing features of tidal fluctuation. The difficulty of intertidal area classification is compounded because a high proportion of this area is frequently flooded by water, making statistical modeling methods with spatial contextual information often ineffective. Because polarimetric entropy and anisotropy play significant roles in characterizing intertidal areas, in this paper we propose a novel unsupervised contextual classification algorithm. The key point of the method is to combine the generalized extreme value (GEV) statistical model of the polarization features and the Markov random field (MRF) for contextual smoothing. A goodness-of-fit test is added to determine the significance of the components of the statistical model. The final classification results are obtained by effectively combining the results of polarimetric entropy and anisotropy. Experimental results of the polarimetric data obtained by the Chinese Gaofen-3 SAR satellite demonstrate the feasibility and superiority of the proposed classification algorithm.

Keywords: Intertidal classification; Polarimetric synthetic aperture radar; Finite mixture model; Markov random field; Generalized extreme value model
https://doi.org/10.1631/FITEE.1700462 **CLC number:** TP75

1 Introduction

The intertidal area is a special kind of coastal area due to its rapidly and dramatically changing features caused by the regularly changing water levels and the ebb and flood of tidal water (Lee et al., 2011). Because of their unique properties, intertidal areas possess a high application value, and can be used in underwater cultivation, coastal defense, economic exploitation, etc. For this reason, much attention has been paid by authorities and satellite-based industries globally on monitoring and studying the intertidal area (Inglada and Garello, 2000; Li, 2009; Kim et al., 2011; Won et al., 2013). One of the most important tasks is to classify different regions in the intertidal area with a high accuracy based on remote sensing images. Synthetic aperture radar (SAR) has been proven powerful in intertidal area related studies. Among all the SAR modes, polarimetric SAR (PolSAR) has attracted enormous research effort in satellite-based real-world applications, because it can provide detailed information on the observed target, compared with other SAR modes (Kim et al., 2009; Park et al., 2009; Li et al., 2014).

‡ Corresponding author

* Project supported by the National Natural Science Foundation of China (No. 61331017)

ORCID: Ting-ting JIN, http://orcid.org/0000-0003-3712-1562; Xiao-qiang SHE, http://orcid.org/0000-0003-3063-770X

Nowadays, there are two types of classification method for the intertidal area in PolSAR images. One type is based on multi-polarization features, and the other is based on statistical properties. Multi-polarization features can provide a new perspective for using PolSAR data because the PolSAR system can simultaneously obtain four-channel data of the observed region by transmitting and receiving linear polarization pulses in pairs of four combinations of linear horizontal (H) and vertical (V) polarizations (Boerner, 1990). From the four-channel PolSAR data, multi-polarization features describing physicochemical properties and scattering behavior of the target surface can be extracted using scattering decomposition and eigenvalue analysis (Cloude and Pottier, 1996). Hence, a series of methods based on multi-polarization features have been proposed and verified in recent years. These methods, such as the Cloude decomposition-based framework proposed by Cloude and Poitter (1996) and the polarimetric entropy-based target extraction method proposed by Cloude (1995), have been applied in terrain classification and target extraction. The second type of method is based on the statistical properties of the PolSAR data in dealing with terrain classification. These methods are based mainly on the finite mixture model (FMM) theory. FMMs, including the traditional Wishart mixture model (Wu et al., 2008) and some non-Gaussian mixture models (Doulgeris et al., 2012), are widely used in urban area classification, sea-land segmentation, and farmland monitoring.

However, classification of the intertidal area in PolSAR images is not a simple task, because there are similar electromagnetic scatter mechanisms between the sea surface and the intertidal area, which are composed mainly of underwater cultivation, remnant water bodies, aquatic farms, etc. Moreover, components of the intertidal area, such as underwater cultivation and remnant water bodies, have similar scatter intensities in the SAR image, and are thus difficult to distinguish. Therefore, most state-of-the-art classification methods cannot be used in classifying intertidal areas. Existing studies of the intertidal area focus mainly on applications such as topographic change detection (Li et al., 2012, 2013), soil moisture analyses (Kim et al., 2009), and scattering mechanism analyses for some special targets (van del Wal et al., 2005; Won et al., 2013; Geng et al., 2016), but pay little attention to the classification work. She (2017) proposed a novel classification method by combining the generalized extreme value mixture models (GEVMMs) and the expectation–maximization (EM) algorithm. This approach can obtain good classification performance for the intertidal areas, which have distinct boundaries. However, a small margin of noise will arise without smoothing filtering when the area is more complicated.

In this paper, we propose an integrated classification approach for the intertidal area combining GEVMM and Markov random fields (MRF). First, through careful inspection of intertidal area PolSAR data, we select the two most powerful multi-polarization features, i.e., polarimetric entropy and polarimetric anisotropy, to fully characterize the scattering mechanism. Then, based on the extreme value theory, the generalized extreme value (GEV) distribution is adopted to describe the statistical properties of the selected features (She et al., 2017). Then, a novel classification method is developed for the intertidal area by combining GEVMM and GEV distribution based MRF. When building GEVMM, we use an effective approach to determine whether one of its components is significant. Specifically, the image field of MRF is set by the GEV distribution. Finally, the proposed algorithm is verified using polarimetric data acquired by the Chinese Gaofen-3 satellite. The proposed classification approach has a better discrimination ability for the intertidal area compared with traditional ones.

2 Algorithm description

In this section, we describe the proposed integrated classification approach for the intertidal area. This method has three steps. The first step is selecting the most promising features, i.e., polarimetric entropy and anisotropy, to fully characterize the intertidal area. Then, we propose an automatic classification algorithm that includes building mixture models and the MRF model based on statistical analysis of the selected features. The final classification result is achieved by combining the results of different features. The flowchart of the proposed method is given in Fig. 1.

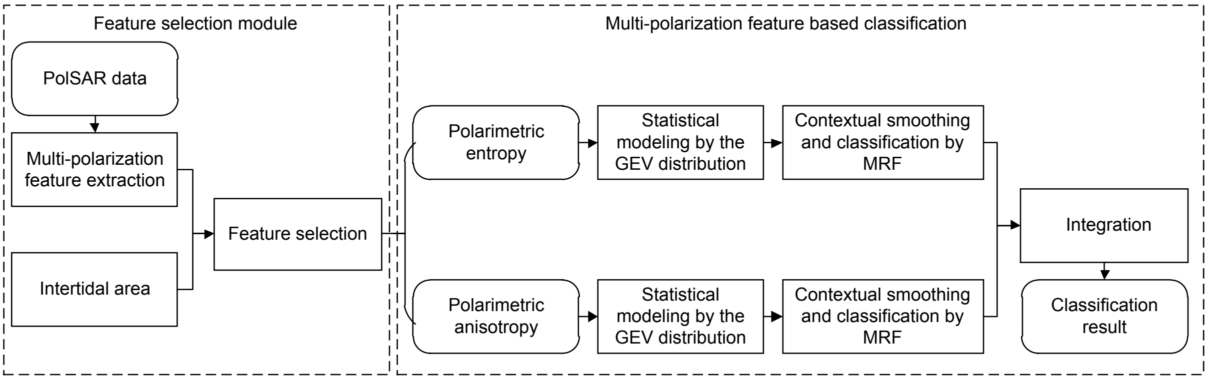

Fig. 1 Flowchart of the proposed method (GEV: generalized extreme value; MRF: Markov random field)

2.1 Synthetic aperture radar polarimetry and multi-polarization feature analysis

PolSAR data can offer a different way to describe the observed scene surface by methods that exploit the combined information of the back-scattering coefficients, among which the most famous is $H/A/\alpha$ decomposition. The definition of $H/A/\alpha$ decomposition is based on the polarimetric coherency $\boldsymbol{T}_3$ matrix (Pottier, 1998):

$$\boldsymbol{T}_3=\sum_{i=1}^{3}\lambda_i\boldsymbol{T}_{3i}=\sum_{i=1}^{3}\lambda_i\boldsymbol{u}_i\boldsymbol{u}_i^{\mathrm{H}}, \tag{1}$$

where real numbers λ_i (i=1, 2, 3) are the eigenvalues of $\boldsymbol{T}_3$, representing statistical weights for the i^{th} normalized component target $\boldsymbol{T}_{3i}$, occurring with pseudo-probabilities P_i, given by

$$P_i=\lambda_i\Big/\sum_{i=1}^{3}\lambda_i. \tag{2}$$

Polarimetric entropy H and anisotropy A can be calculated by eigenvalues λ_i and their corresponding pseudo-probabilities P_i (Pottier, 1998):

$$H=-\sum_{i=1}^{3}P_i\log P_i, \tag{3}$$

$$A=\frac{\lambda_2-\lambda_3}{\lambda_2+\lambda_3}. \tag{4}$$

The mean scatter angle α is an important multi-polarization feature. It can be computed from the eigenvectors as

$$\alpha=\sum_{i=1}^{3}P_i\arccos\left|\boldsymbol{u}_i(1)\right|, \tag{5}$$

where the mean scatter angle α varies between 0° and 90°, and $\boldsymbol{u}_i(1)$ is the eigenvector.

Among the multi-polarization features extracted from the combined information of the four-channel PolSAR images, Span is an efficient parameter to describe all information related to the total power:

$$\text{Span}=\left|S_{\mathrm{HH}}\right|^2+\left|S_{\mathrm{HV}}\right|^2+\left|S_{\mathrm{VH}}\right|^2+\left|S_{\mathrm{VV}}\right|^2. \tag{6}$$

Span contains all the details in the four-channel POLSAR images.

Fig. 2 gives examples of the above four features of the intertidal area. According to their definitions, the range of polarimetric entropy and anisotropy is 0 and 1, and the mean scatter angle α is normalized as 0°–90°. To obtain a fair comparison, the total power of Span is also normalized between 0 and 1. In the intertidal area, flooded aquatic farms, i.e., shallow water area, mudflats, aquatic farms exposed to air, and other types of objects, form a complex environment. Among them, the mudflats and shallow water area have a relatively smooth surface. Therefore, some parts of the intertidal area have a similar magnitude value in the PolSAR amplitude images compared with the sea surface. Consequently, the total power of Span (Fig. 2a) cannot clearly distinguish the sea from the intertidal area.

The complex environment of the intertidal area leads to a complicated polarization-dependent texture distribution. This distribution is closely correlated to scatter randomness, which can be measured by polarimetric entropy H and its complementary feature,

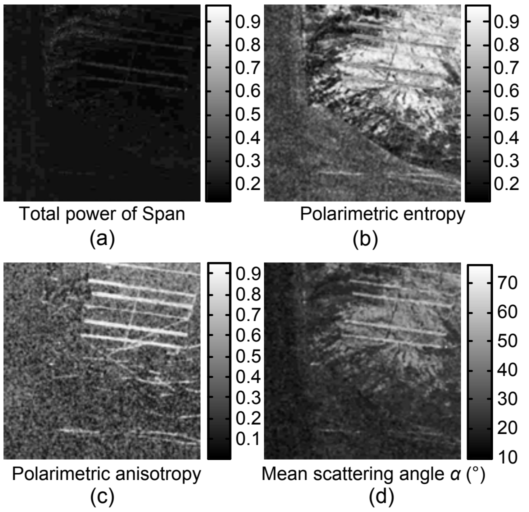

Fig. 2 Examples of the features of the intertidal area: (a) total power of Span; (b) polarimetric entropy; (c) polarimetric anisotropy; (d) mean scattering angle

polarimetric anisotropy A. Examples of polarimetric entropy and anisotropy are given in Figs. 2b and 2c. Compared with Span (Fig. 2a), polarimetric entropy can distinguish the sea surface and different types of land covers in the intertidal area, and polarimetric anisotropy can distinguish regions with high entropy. Therefore, using these two features, we can fully characterize the intertidal area.

The mean scatter angle α describes the underlying average physical scattering mechanism directly. The lower value occurs over targets with smooth surfaces, while the higher value represents targets with volume scattering and double bounce scattering as the value increases. The mean scatter angle α can measure the surface roughness of the intertidal area. Targets such as mudflats and water bodies differ in α due to different surface roughness (Fig. 2d). However, the tidal force results in a relatively smooth appearance of the intertidal area, representing a surface scattering mechanism. Therefore, there is difficulty in classifying the intertidal area that has the mean scatter angle α.

From the analysis above, polarimetric entropy and anisotropy are selected from the four-polarization features to describe the intertidal area.

2.2 Statistical modeling by the generalized extreme value distribution

Generally, most parts of the intertidal area have relatively low entropy values, although extreme cases may occur in regions such as the mudflats and some parts of the aquatic farm area, where some branches of underwater vegetation may be exposed to air. These high entropy values lead to a "long-tail" phenomenon in the histogram. The long-tail phenomenon is also significant in the polarimetric anisotropy image, because it easily reaches an extremely high value when the polarimetric entropy value increases. The long-tail phenomenon plays an important role in studies of extreme events such as risk prediction and disaster warning. There are two forms of the long-tail phenomenon, i.e., the left tail and the right tail. Current models, including the Gaussian and Gamma models, cannot provide satisfactory fitting results for histograms with the long-tail phenomenon (Ding et al., 2015). Models used commonly to describe the long-tail phenomenon, such as the generalized Gamma distribution and the K-distribution, can describe the right tail well; however, they cannot adapt to the left tail. Moreover, the K-distribution, which is proposed based on the multiplicative noise model, is used mainly to describe relatively homogeneous regions and may not be suitable for images with complicated textures such as polarimetric entropy images and polarimetric anisotropy images (Li et al., 2007).

Based on the extreme value theory, the GEV distribution is helpful in describing the long-tail phenomenon and has been used widely in SAR image-based applications (Won et al., 2013). Therefore, the GEV distribution is adopted to model the polarimetric entropy and anisotropy images of the intertidal area in this study. The probability density function (PDF) of the GEV distribution is defined as (Ding et al., 2015)

$$\mathrm{gev}(x,\mu,\sigma,\xi)=\frac{1}{\sigma}\exp\left(-\left(\xi\frac{x-\mu}{\sigma}+1\right)^{-\frac{1}{\xi}}\right)\cdot\left(\xi\frac{x-\mu}{\sigma}+1\right)^{-1-\frac{1}{\xi}}, \tag{7}$$

where ξ, σ, and μ are the three parameters that characterize the GEV distribution, which are the shape, scale, and location, respectively. The shapes of the GEV distributions change depending on the positive or negative of ξ. Fig. 3 shows the shapes of the GEV distribution with three types of shape parameter ξ.

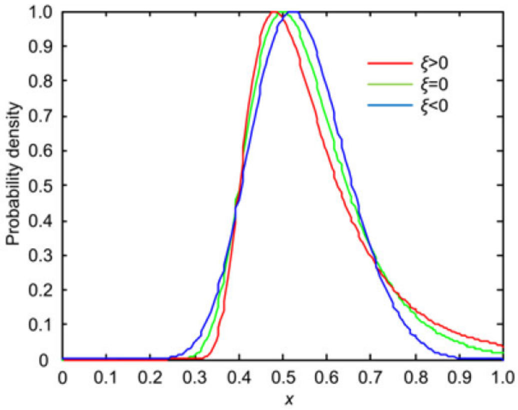

Fig. 3 Probability densities of the three types of generalized extreme value distribution (References to color refer to the online version of this figure)

Through the above analysis, the GEV model has been proven effective in describing the statistical properties of the polarimetric entropy and anisotropy image over the intertidal area. Considering the complexity of the intertidal area, we propose a novel GEVMM to fully characterize the intertidal area based on the FMM theory:

$$f(x;\xi,\sigma,\mu)=\sum_{i=1}^{n}a_i f_i(x;\xi_i,\sigma_i,\mu_i), \tag{8}$$

where n indicates the class of the intertidal area, and $f_i(\cdot)$ represents the i^{th} GEV model. Based on Eq. (8), we build the GEVMM for the polarimetric entropy and anisotropy separately.

When building the GEVMM for polarimetric entropy and anisotropy, the most crucial step is the calculation of parameters of every component. In this study, the calculation of GEVMM is based on the EM algorithm.

The EM algorithm is a maximum likelihood estimation (MLE) algorithm, which can estimate FMM in an iterative way. Each iteration of the algorithm is made up of the E step (calculation of the expectation) and the M step (maximization of the expectation). First, the number of components of GEVMM is initialized. Then in the E step we calculate responses $\hat{\gamma}_{ji}$ from the i^{th} GEV model for the j^{th} pixel as

$$\hat{\gamma}_{ji}=\frac{a_i f_i\left(x_j;\xi_i,\sigma_i,\mu_i|\theta_i\right)}{\sum_{i}^{n}a_i f_i\left(x_j;\xi_i,\sigma_i,\mu_i|\theta_i\right)}, \tag{9}$$

where $j\in\{0, 1, \ldots\}$ is the label for the pixel, i is the class label, and θ_i indicates the i^{th} class. Afterwards, in the M step, pixels are labeled as i by the maximum response $\hat{\gamma}_{ji}$, and new parameters are estimated by MLE. In our experiment, the estimation was achieved by MATLAB function gevfit. The iterative process continued until the parameters converged around a constant value.

On the other hand, the fixed number of components of the traditional FMM makes it difficult to describe the complex environment of the intertidal area. Therefore, an adaptive estimation method is proposed in this study to determine whether a component of GEVMM is significant. In the iteration, the significance of each component is determined by the number of pixels contained. If the number is lower than a given threshold, it indicates that the pixels are insufficient to build a significant GEV model, and should be removed. In our experiment, the threshold was set at 50.

After the iterative process converged, GEVMM was built. Based on the GEVMM, each pixel of the image can be classified to a specific component, and a label map was obtained.

2.3 Markov random fields

In this subsection, we introduce MRF to contextually smooth the label map from GEVMM. MRF modeling takes the class memberships of spatially neighboring classes into account using an isotropic second-order neighborhood system (Li, 2009). When building MRF, we use the GEV mixture models to calculate the prior probabilities along with the Potts model. For the j^{th} pixel, the prior probabilities of the i^{th} class can be given by

$$P(x_j\mid i)=f_i(x_j;\xi_i,\sigma_i,\mu_i)\pi_i^{(j)}, \tag{10}$$

where $\pi_i^{(j)}$ is the Potts model:

$$\pi_i^{(j)}=\frac{\exp\left(\beta m_i^{(j)}\right)}{\sum_{l=1}^{k}\exp\left(\beta m_l^{(j)}\right)}, \tag{11}$$

where $m_i^{(j)}$ is the number of pixels in the neighborhood of x_i, and β is a positive constant measuring the correlation of the pixels in current neighborhoods. β

was set as 1 in our experiments.

The workflow integrating GEVMM and MRF is given in Fig. 4 with detailed descriptions.

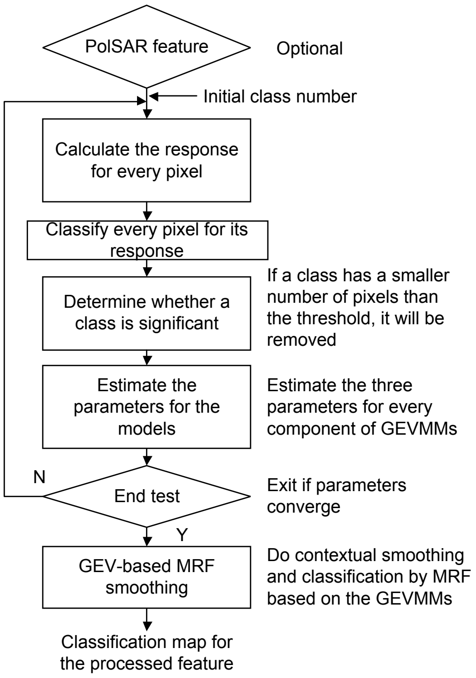

Fig. 4 Workflow of the integration of GEVMM and MRF
GEV: generalized extreme value; GEVMM: GEV mixture model; MRF: Markov random field

2.4 Combining the classification results

Based on the workflow (Fig. 4), two classification results can be obtained for polarimetric entropy and anisotropy. To obtain a better final result, the two classification results are combined. Assuming that the classification result of the polarimetric entropy containing M classes is $\{A_1, A_2, \ldots, A_M\}$, and that of the polarimetric anisotropy containing N classes is $\{B_1, B_2, \ldots, B_N\}$, their intersection can be given as

$$C=\left\{A_i \cap B_j,\ A_i \cap B_j \neq \varnothing,\ i\in[1,M],\ j\in[1,2]\right\}. \quad (12)$$

This method aims to determine the ownership of an element of their intersection. For every pixel x in C, the attribution for classes A_i and B_j can be defined as

$$\begin{cases} m_x(A_i)=\left|H(x)-x_{A_i}\right|, & (13) \\ m_x(B_j)=\left|A(x)-x_{B_j}\right|, & (14) \end{cases}$$

where $H(x)$ is the value in the polarimetric entropy for pixel x, and x_{A_i} is the mean value of the pixels that belong to class A_i, i.e., the class center. Similarly, $A(x)$ is the value in the polarimetric anisotropy for pixel x, and x_{B_j} is the mean value of the pixels that belong to class B_j. When $\sum_{x\in C} m_x(A_i) > \sum_{x\in C} m_x(B_j)$, C belongs to class A_i; otherwise, C belongs to B_j. By combining the two classification maps in this way, the final classification result is achieved.

3 Experiments and analysis

The proposed classification method was evaluated and validated by the Gaofen-3 quad-polarization data over the intertidal area in Rudong, Jiangsu Province, China. The resolution of the experimental data was 8 m. The acquisition time was December 31, 2016 at the ebb tide. Fig. 5 shows the Pauli image of the PolSAR data, where the study area is marked as the yellow frame and measures 12 km×8 km.

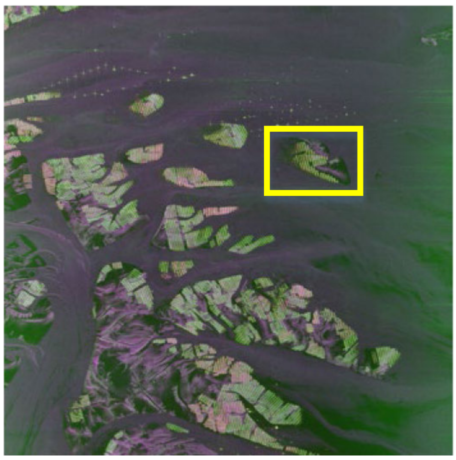

Fig. 5 The Pauli image of the quad-polarization data over the intertidal area in Rudong, Jiangsu Province, China
The yellow box contains the region used in the experiment. References to color refer to the online version of this figure

Our experiment was made up of three steps: (1) The multi-polarization features analyzed in Section 2.1 were validated visually and quantitatively; (2) The study area was classified based on the flowchart shown in Fig. 1; (3) A comparison experiment was carried out with the Wishart-$H/A/\alpha$ method.

3.1 Feature selection

Fig. 6 demonstrates the four multi-polarization features of the study area selected in the yellow box shown in Fig. 5. Based on the Pauli image, we analyzed these four features visually. In the Span image given in Fig. 6a, the contour of the intertidal area can be obtained, but the details are indistinguishable. In addition, the edges between the intertidal area and the sea are not clear in the Span image. The polarimetric entropy (Fig. 6b) can discriminate the mudflats and both the flooded and exposed parts of the aquatic farms in the intertidal area that is visible. In the polarimetric entropy image, the contrast between the sea surface and the intertidal area is also obvious. Fig. 6c shows the polarimetric anisotropy image, in which we can clearly recognize the mudflats, although the mean scattering angle α (Fig. 6d) has relatively poor discrimination ability for the study area. Among these four figures, it can be seen that polarimetric entropy has the best visual discrimination ability and polarimetric anisotropy plays a complementary role. Therefore, the combination of polarimetric entropy and anisotropy can offer the best interpretation result for the area of interest.

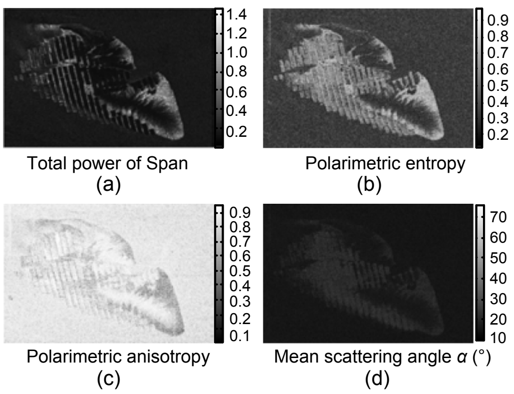

Fig. 6 Multi-polarization features of the study area: (a) total power of Span; (b) polarimetric entropy; (c) polarimetric anisotropy; (d) mean scattering angle

We evaluate these features by between-region contrasts using the Michelson contrast. The Michelson contrast has been used widely in evaluating SAR images (Peli, 1990), given as

$$C = \frac{F_{\max} - F_{\min}}{F_{\max} + F_{\min}}, \tag{15}$$

where $F_{\max}$ and $F_{\min}$ are the maximum and minimum feature values, respectively, and C indicates the contrast value between 0 and 1. The increasing C values indicate better discrimination abilities. Table 1 shows the contrast values of the four features. Among them, polarimetric entropy has the highest contrast value and polarimetric anisotropy follows. According to the analysis in Section 2.1, polarimetric anisotropy is valuable in describing the regions with high entropy values in the intertidal area, for instance, the mudflats, as described in Fig. 6c. Polarimetric entropy can describe the details of the intertidal area and offers the best discrimination capability. The mean scatter angle α fails in the intertidal area with relatively low contrast areas. Span, however, has the poorest discrimination ability.

Table 1 The Michelson contrast measure for different features

Feature	Michelson contrast value
Span	0.6721
Polarimeric entropy	0.9585
Polarimetric anisotropy	0.9176
Mean scattering angle α	0.8216

3.2 Statistical modeling and fitting test

Based on the workflow given in Fig. 4, we built the GEVMM for polarimetric entropy and anisotropy. Initially, there were five components for the polarimetric entropy GEVMM and two for the polarimetric anisotropy GEVMM. After iterations, the final number of the components was three and two, respectively. Fig. 7 demonstrates the viability of GEVMM for polarimetric entropy. To ensure the superiority of GEVMM, the Gamma and log-normal distributions were also used to fit the histogram of each component of GEVMM. Figs. 7a–7c show the fitting results. Compared with the Gamma distribution and the log-normal distribution, the GEV distribution demonstrates a better fitting result in Fig. 7a, especially for the left-tail phenomenon. The component in Fig. 7b describes mainly the underwater cultivation area, i.e., the shallow water area. This area is relatively small and not obvious in the statistical characteristics, so deviations exist in the fitting results. In Fig. 7d, GEVMM has a good consistency with the histogram of polarimetric entropy.

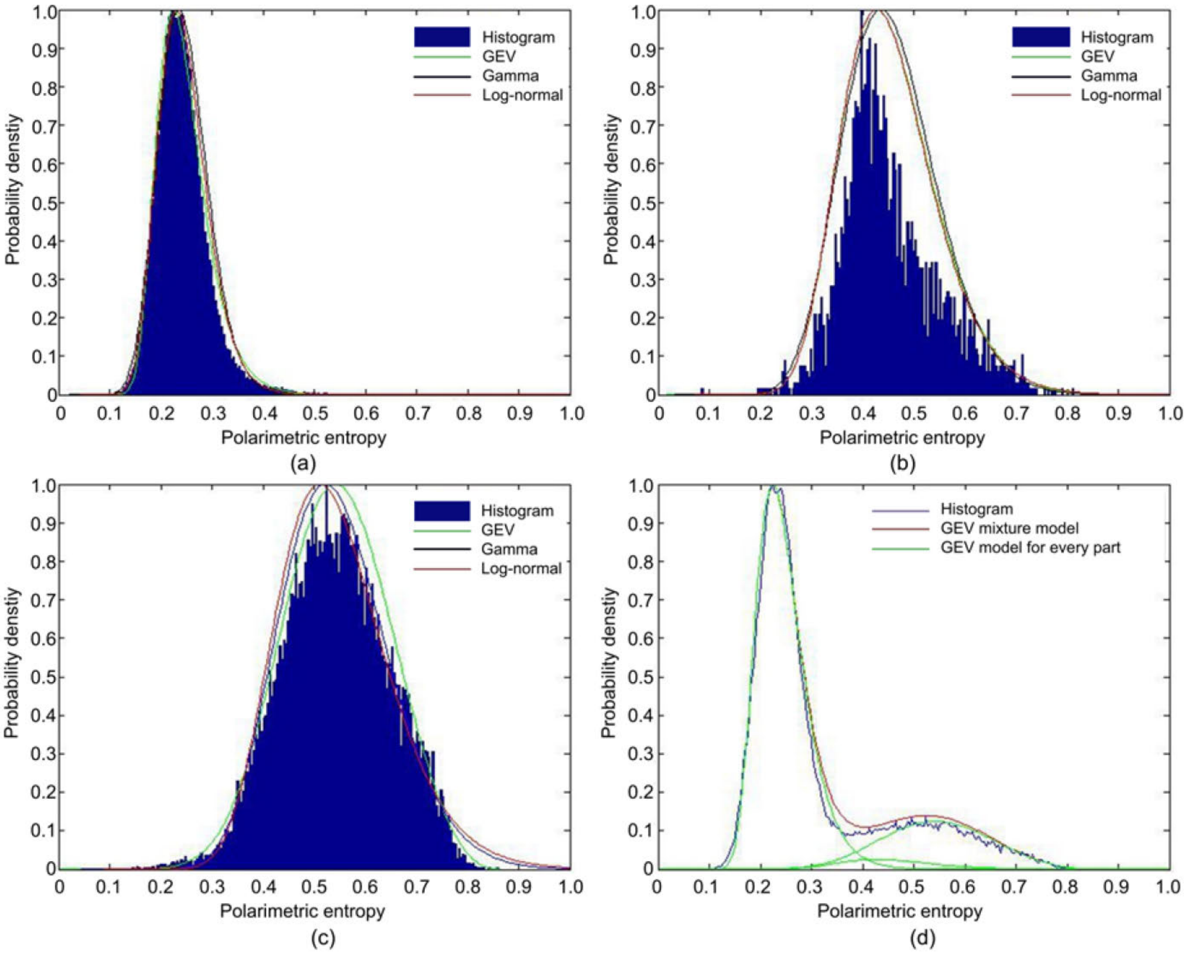

Fig. 7 Fitness comparison among the GEV, Gamma, and log-normal distributions of components 1 (a), 2 (b), and 3 (c) in the polarimetric entropy GEVMM, and the distribution results obtained by different models (d)
GEV: generalized extreme value; GEVMM: GEV mixture model. References to color refer to the online version of this figure

Similarly, the number of components is initialized as two when building the polarimetric anisotropy GEVMM. After the iteration, the final number of the components is two. The final results are illustrated in Fig. 8, which shows that the GEV distribution outperforms the Gamma and log-normal distributions. Moreover, GEVMM agrees well with the histogram of polarimetric anisotropy. To further measure the fitness, the Akaike information criterion (AIC) was employed to validate the GEVMM we obtained (Akaike, 1973). The definition of AIC is given as

$$\mathrm{AIC}=\frac{2k-2L}{n}, \tag{16}$$

where k is the number of parameters, n is the number of samples, and L is the log-likelihood. The log-likelihood is defined by

$$L=-\frac{n}{2}\ln(2\pi)-\frac{n}{2}\ln\left(\frac{\mathrm{sse}}{n}\right)-\frac{n}{2}, \tag{17}$$

where sse is the sum of the squared residuals between PDFs and histograms. The smaller the k or the larger the L, the smaller the AIC. This means that the smaller the k, the more concise the model, and the larger the L, the more accurate the model. AIC values of the three distributions shown in Figs. 7 and 8 are given in Tables 2 and 3, respectively, where we can see that the GEV distribution is superior to the other two distributions. Combining Figs. 7 and 8 and Tables 2 and 3, we can conclude that the GEV distribution has the

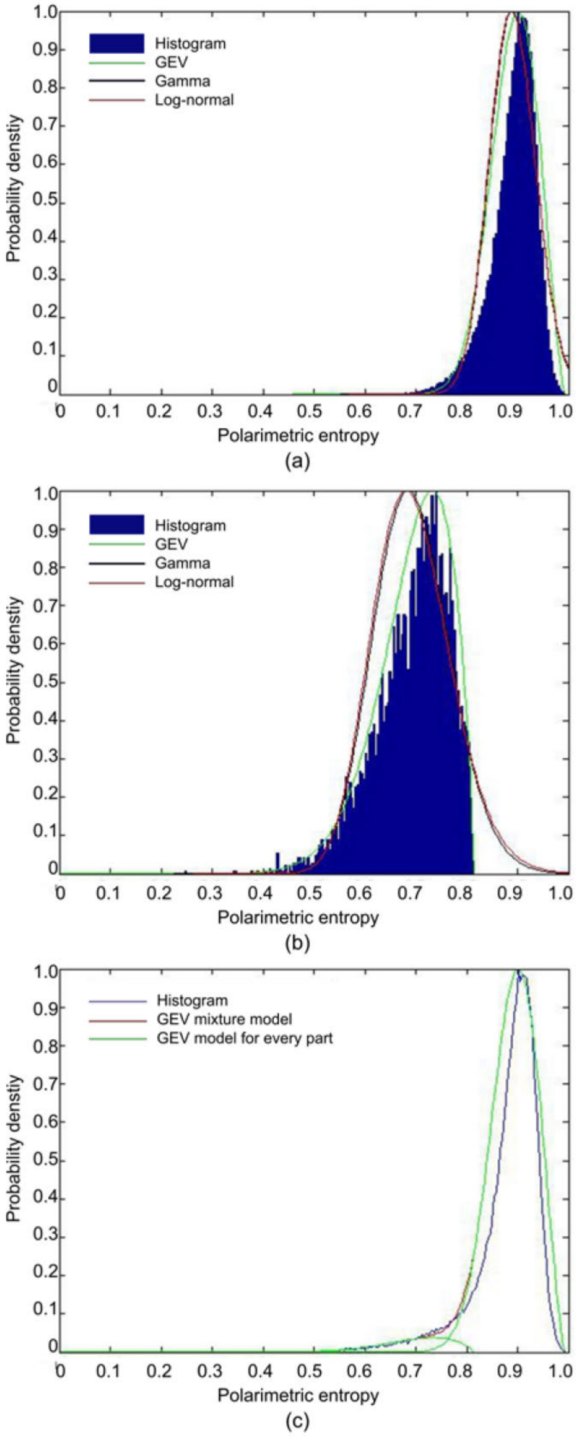

Fig. 8 Fitness comparison among the GEV distribution, Gamma distribution, and log-normal distribution of components 1 (a) and 2 (b) in the polarimetric anisotropy GEVMM, and the distribution results obtained by different models (c)

GEV: generalized extreme value; GEVMM: GEV mixture model. References to color refer to the online version of this figure

Table 2 The AIC values of the fitting results among the GEV, Gamma, and log-normal distributions for the three classes of polarimetric entropy

Distribution	AIC value		
	Case 1	Case 2	Case 3
GEV	5.3846	5.2856	4.5271
Gamma	10.3163	6.1584	8.1451
Log-normal	10.3162	6.1557	8.1454

AIC: Akaike information criterion; GEV: generalized extreme value; GEVMM: GEV mixture model

Table 3 The AIC values of the fitting results among the GEV, Gamma, and log-normal distributions for the two classes of polarimetric anisotropy

Distribution	AIC value	
	Case 1	Case 2
GEV	6.1658	4.2192
Gamma	10.6635	7.2673
Log-normal	10.6633	7.2689

AIC: Akaike information criterion; GEV: generalized extreme value; GEVMM: GEV mixture model

best fitting ability. In addition, the final GEVMMs of the polarimetric entropy and anisotropy are validated by the AIC values 4.9701 and 4.8023, respectively.

3.3 Classification results

Based on the GEVMMs of polarimetric entropy and anisotropy, we applied the MRF introduced in Section 2.3 to obtain their classification results; the final result was obtained by combining the two classification results, as given in Fig. 9. Fig. 9a illustrates the Pauli image of the study area. The classification results from polarimetric entropy and anisotropy are given in Figs. 9b and 9c, where the study area is classified into three classes based on polarimetric entropy, and into two classes based on polarimetric anisotropy. Compared with the ground truth given in Fig. 9f, the classification results derived from polarimetric entropy discriminate the sea area and the aquatic farm area well, but are incapable of distinguishing the aquatic farm area from the mudflats. Meanwhile, the results based on polarimetric anisotropy can extract the mudflats well. The proposed method was applied with the two classification results in Figs. 9b and 9c to obtain the final classification result.

The three classes from polarimetric entropy can be given as $\{A_1, A_2, A_3\}$, and the two classes from polarimetric anisotropy can be given as $\{B_1, B_2\}$.

Then their intersections can be given as $C=\{A_i\cap B_j, A_i\cap B_j\neq\Phi, i\in\{1, 2, 3\}, j\in\{1, 2\}\}$. In this experiment, the two classification results have six intersections, given as $C=\{C_k, k\in\{1, 2, \ldots, 6\}\}$. Based on the integration process given in Fig. 4, every C_k can be labeled by A_i or B_j, considering the attributions of the pixels in it. When all the intersections are labelled, the final classification result is achieved. Fig. 9d shows the final classification result, which contains four classes, i.e., sea area, flooded aquatic farm, exposed aquatic farms, and mudflats. Compared with Fig. 9f, the final classification result shows a good visual consistency with the ground truth, whereas the comparative result obtained using the Wishart-$H/A/\alpha$ method (Fig. 9e) can discriminate only mudflats and fails to identify other land cover types of the intertidal area. Therefore, our classification algorithm outperforms the Wishart-$H/A/\alpha$ method with a better discrimination ability.

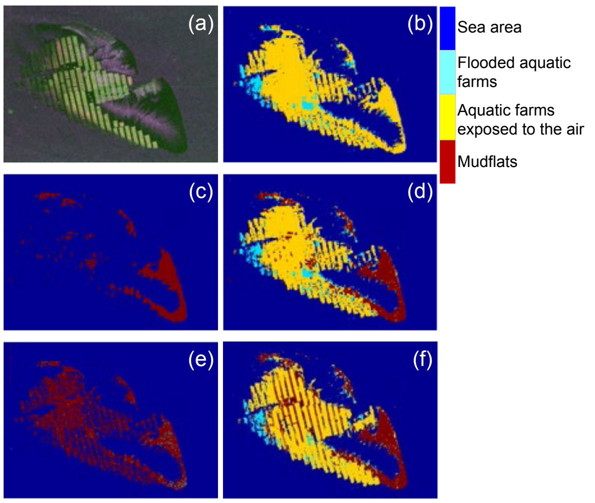

Fig. 9 Comparison of different methods: (a) Pauli image of the study area; (b) classification results with entropy; (c) classification results with anisotropy; (d) results with the proposed approach; (e) results with the Wishart-$H/A/\alpha$ method; (f) ground truth

References to color refer to the online version of this figure

For further validation, we used the Kappa coefficient and the overall accuracy (OA) of classification to evaluate our method (Uebersax, 1982). The results are given in Table 4. The proposed method performed better for these two measurements. Therefore, the proposed approach outperformed the Wishart-$H/A/\alpha$ method both visually and quantitatively.

Table 4 The Kappa coefficient and OA values of the two methods

Method	Kappa coefficient	OA of classification
Proposed	0.9333	0.9254
Wishart-$H/A/\alpha$	0.6532	0.6576

OA: overall accuracy

4 Discussion

In this section, we discuss the reasons for the above experimental results. The main problem of intertidal area classification is the similar scattering mechanism of the objects in the intertidal area and the sea surface. Therefore, it is difficult to label different classes in this area in the four-channel PolSAR images and most of the multi-polarization features. The Wishart-$H/A/\alpha$ method makes full use of the original PolSAR data and the information of three multi-polarization features, i.e., polarimetric entropy, polarimetric anisotropy, and mean scattering angle α. Hence, it is used widely as a strong baseline in PolSAR data based classifications. Although we established in Section 2.1 that polarimetric entropy and anisotropy are the main distinguishing features of intertidal areas in PolSAR imagery due to their sensitivity to scattering randomness, the poor discriminatory ability of the mean scattering angle α and the PolSAR data prevents the Wishart-$H/A/\alpha$ method from achieving satisfactory classification results for intertidal areas.

By employing the FMM theory and MRF, the proposed classification method takes full advantage of the distinguishing features and achieves better classification results.

5 Conclusions

We proposed a novel classification approach for the intertidal area that combines GEV mixture models and the MRF model in PolSAR images. In our study, polarimetric entropy and anisotropy were introduced to fully characterize the intertidal area. An automatic unsupervised contextual classification framework was developed to address the classification problems of the intertidal area using the GEV distribution, which was proven appropriate to describe the statistical properties of the polarimetric and anisotropy images in that area. Specifically, by introducing the FMM theory, two GEVMMs were built based on the GEV distribution to fit the histograms of polarimetric entropy and anisotropy. Furthermore, by using the GEV distribution based MRF, the contextual smoothing work was achieved and two classification maps were obtained. Finally, experiments were conducted with the PolSAR data acquired by the Chinese Gaofen-r3 satellite over the intertidal area in Rudong, Jiangsu Province, China. The proposed approach outperformed the traditional ones in classification considering the ground truth, and thus verified the effectiveness of the proposed method.

The proposed approach has prospects for geographic mapping and land-use classification of intertidal areas. When more influential features are developed to describe intertidal areas, additional adaptive modifications can also be made to improve the performance.

References

Akaike H, 1973. Information theory and an extension of the maximum likelihood principle. Proc 2nd Int Symp on Information Theory, p.267-281.

Boerner WM, 1990. Introduction to radar polarimetry—with assessments of the historical development and of the current state-of-the-art. In: Guran AS, Mittra R, Moser PJ (Eds.), Electromagnetic Wave Interactions. World Scientific, Singapore, p.139-214. https://doi.org/10.1142/9789812813091_0004

Cloude SR, 1995. An entropy based classification scheme for polarimetric SAR data. Int Geoscience and Remote Sensing Symp, p.2000-2002. https://doi.org/10.1109/ IGARSS.1995.524090

Cloude SR, Pottier E, 1996. A review of target decomposition theorems in radar polarimetry. *IEEE Trans Geosci Remote Sens*, 34(2):498-518. https://doi.org/10.1109/36.485127

Ding H, Huang Y, Liu N, et al., 2015. Modeling of sea spike events with generalized extreme value distribution. European Radar Conf, p.113-116. https://doi.org/10.1109/EuRAD.2015.7346250

Doulgeris AP, Akbari V, Eltoft T, 2012. Automatic PolSAR segmentation with the $\mathcal{U}$-distribution and Markov random fields. European Conf on Synthetic Aperture Radar, p.183-186.

Geng XM, Li XM, Velotto D, et al., 2016. Study of the polarimetric characteristics of mud flats in an intertidal zone using C- and X-band spaceborne SAR data. *Remote Sens Environ*, 176:56-68. https://doi.org/10.1016/j.rse.2016.01.009

Inglada J, Garello R, 2000. Underwater bottom topography estimation from SAR images by regularization of the inverse imaging mechanism. Proc IEEE Int Geoscience and Remote Sensing Symp, p.1848-1850. https://doi.org/10.1109/IGARSS.2000.858143

Kim DJ, Park SE, Lee HS, et al., 2009. Investigation of multiple frequency polarimetric SAR signal backscattering from tidal flats. IEEE Int Geoscience and Remote Sensing Symp, p.896-899. https://doi.org/10.1109/IGARSS.2009.5417916

Kim JE, Park SE, Kim DJ, et al., 2011. Recent advances in POL(in)SAR remote sensing and stress-change monitoring of wetlands with applications to the Sunchon Bay Tidal Flats. European Conf on Synthetic Aperture Radar, p.1-3.

Lee H, Chae H, Cho SJ, 2011. Radar backscattering of intertidal mudflats observed by Radarsat-1 SAR images and ground-based scatterometer experiments. *IEEE Trans Geosci Remote Sens*, 49(5):1701-1711. https://doi.org/10.1109/TGRS.2010.2084094

Li HC, Hong W, Wu YR, 2007. Generalized gamma distribution with MoLC estimation for statistical modeling of SAR images. 1st Asian and Pacific Conf on Synthetic Aperture Radar, p.525-528. https://doi.org/10.1109/APSAR.2007.4418665

Li SZ, 2009. Markov Random Field Modeling in Image Analysis. Springer, London, UK. https://doi.org/10.1007/978-1-84800-279-1

Li Z, Heygester G, Notholt J, 2012. Topographic mapping of Wadden Sea, with SAR images and waterlevel model data. IEEE Int Geoscience and Remote Sensing Symp, p.2645-2648. https://doi.org/10.1109/IGARSS.2012.6350385

Li Z, Heygester G, Notholt J, 2013. The topography comparsion between the year 1999 and 2006 of German tidal flat wadden sea analyzing SAR images with waterline method. IEEE Int Geoscience and Remote Sensing Symp, p.2443-2446. https://doi.org/10.1109/IGARSS.2013.6723314

Li Z, Heygster G, Notholt J, 2014. Intertidal topographic maps and morphological changes in the German wadden sea between 1996–1999 and 2006–2009 from the waterline method and SAR images. *IEEE J Sel Top Appl Earth Observ Remote Sens*, 7(8):3210-3224. https://doi.org/10.1109/JSTARS.2014.2313062

Park SE, Moon WM, Kim DJ, 2009. Estimation of surface roughness parameter in intertidal mudflat using airborne polarimetric SAR data. *IEEE Trans Geosci Remote Sens*, 47(4):1022-1031. https://doi.org/10.1109/TGRS.2008.2008908

Peli E, 1990. Contrast in complex images. *J Opt Soc Am A*, 7(10):2023-2040. https://doi.org/10.1364/JOSAA.7.002032

Pottier E, 1998. Unsupervised classification scheme and topography derivation of POLSAR data on the *H*/*A*/*a* polarimetric decomposition theorem. Proc 4th Int Workshop

on Radar Polarimetry, p.535-548.
She X, Qiu X, Lei B, et al., 2017. A classification method based on polarimetric entropy and GEV mixture model for intertidal area of PolSAR image. *J Rad*, 6(5):554-563 (in Chinese). https://doi.org/10.12000/JR16149
Uebersax JS, 1982. A generalized Kappa coefficient. *Educ Psychol Meas Sage Publ*, 42(1):181-183. https://doi.org/10.1177/0013164482421018
van del Wal D, Herman PMJ, van den Dool AW, 2005. Characterisation of surface roughness and sediment texture of intertidal flats using ERS SAR imagery. *Remote Sens Environ*, 98(1):96-109. https://doi.org/10.1016/j.rse.2005.06.004 https://doi.org/10.1109/IGARSS.2011.6049578
Won ES, Ouchi K, Yang CS, 2013. Extraction of underwater laver cultivation nets by SAR polarimetric entropy. *IEEE Geosci Remote Sens Lett*, 10(2):231-235. https://doi.org/10.1109/LGRS.2012.2199077
Wu Y, Ji K, Yu W, et al., 2008. Region-based classification of polarimetric SAR images using Wishart MRF. *IEEE Geosci Remote Sens Lett*, 5(4):668-672. https://doi.org/10.1109/LGRS.2008.2002263